SEISMIC BEHAVIOUR OF A REPAIRED SUPERELASTIC SHAPE MEMORY ALLOY (SMA) REINFORCED CONCRETE BEAM-COLUMN JOINT

Moncef Nehdi[1], M. Shahria Alam and Maged A. Youssef

Department of Civil and Environmental Engineering, The University of Western Ontario, London, ON Canada, N6A5B9

ABSTRACT

Large-scale earthquakes pose serious threats to infrastructure causing substantial damage and large residual deformations. Superelastic (SE) Shape-Memory-Alloys (SMAs) are unique alloys with the ability to undergo large deformations, but can recover its original shape upon stress removal. The purpose of this research is to exploit this characteristic of SMAs such that concrete Beam-Column Joints (BCJs) reinforced with SMA bars at the plastic hinge region experience reduced residual deformation at the end of earthquakes. Another objective is to evaluate the seismic performance of SMA Reinforced Concrete BCJs repaired with flowable Structural-Repair-Concrete (SRC). A ¾-scale BCJ reinforced with SMA rebars in the plastic-hinge zone was tested under reversed cyclic loading, and subsequently repaired and retested. The joint was selected from an RC building located in the seismic region of western Canada. It was designed and detailed according to the NBCC 2005 and CSA A23.3-04 recommendations. The behaviour under reversed cyclic loading of the original and repaired joints, their load-storey drift, and energy dissipation ability were compared. The results demonstrate that SMA-RC BCJs are able to recover nearly all of their post-yield deformation, requiring a minimum amount of repair, even after a large earthquake, proving to be smart structural elements. It was also shown that the use of SRC to repair damaged BCJs can restore its full capacity.

Keywords: beam-column joint, seismic, shape memory alloy, superelasticity, plastic hinge, repair, reversed cyclic loading.

[1] Corresponding Author: Tel: 1-519-661-2111, Ext. 88308, Fax: 1-519-661-3779, Email: mnehdi@eng.uwo.ca.

1. Introduction

The performance of Beam-Column Joints (BCJs) has a considerable influence on the overall behaviour of Reinforced Concrete (RC) moment resisting frames under lateral loads (Engindeniz et al. 2005; Said 2009). Since the 1970's, design codes started enforcing stricter seismic provisions for the detailing of reinforcing bars in beam-column joints realizing its extreme vulnerability during earthquakes (Saatcioglu et al. 2001; Uma and Jain 2006). A considerable number of researchers devoted significant efforts to study the seismic behaviour of RC BCJs in order to develop design recommendations and ensure adequate connection behaviour in RC frame structures. The design of ductile moment-resisting frames aims at forcing the structure to respond in a strong column-weak beam action in which plastic hinges induced by seismic forces form in beams away from the face of the columns. The hinging regions are detailed to allow plastic hinges to undergo yielding under both positive and negative moments, thus ensuring a substantial amount of energy dissipation during earthquakes.

Under strong ground motion, BCJs designed according to current seismic code provisions can dissipate earthquake energy through yielding of the reinforcement and its inelastic deformation. Structures are expected to undergo severe damage, which means saving lives at the expense of incurring substantial economic losses. Repairing such structures is often impractical and/or too costly. Recently, designers/owners have been changing their vision as they no longer accept to surrender their creations/constructions. The seismic design of structures has evolved towards a performance-based approach in which there is need for new structural members and systems that possess enhanced deformation capacity and ductility, higher damage tolerance, decreased residual crack sizes, and recovered or reduced permanent deformations (Parra-Montesinos et al. 2005). Such structures will require a minimum amount of repairing in order to make it serviceable.

Over the last two decades substantial research has been done on the possible uses of SMAs in structural applications (for instance, Alam et al. 2005, 2007a, b and d). If Superelastic (SE) SMAs are used as reinforcing bars, such elite materials can undergo large inelastic deformations and recover their original shape upon stress removal, thus mitigating the problem of permanent deformations. Indeed, when used as reinforcement in critical RC structural elements, SMAs can yield under strains caused by seismic loads, but potentially recover deformations at the end of earthquake events (Saiidi and Wang 2006, Youssef et al. 2008, and Alam et al. 2007c and Alam et al. 2008). Such structural elements will require a minimum amount of repair work (Saiidi and Wang 2006). The properties of SMAs including their high strength, large energy hysteretic behaviour, full recovery of strains up to 8%, high resistance to corrosion and fatigue make them strong contenders for use in earthquake resistant structures (Wilson and Wesolowsky 2005). In particular, Ni-Ti alloy has been found to be the most promising SMA for seismic applications (Alam et al. 2007d).

The present paper reports the results of an experimental study that investigates the effects of using SE SMA bars as reinforcement on the seismic performance of exterior BCJs, as well as on their seismic behaviour after repair. The BCJ specimens have been designed and constructed according to current seismic design standards (NBCC 2005, and CSA A23.3-04), and tested under reversed cyclic loading. The prime objective of this study is to develop a smart concrete BCJ reinforced with SE SMA in its plastic hinge region and investigate its performance under reversed cyclic loading when intact and after repair, and then compare the behaviour of the original to that of the repaired specimen in terms of load-displacement, energy dissipation capacity, and strains in the longitudinal and transverse reinforcements.

2. Research Significance

Conventional steel-RC structures are designed to dissipate energy by yielding of steel during earthquakes, and often suffer permanent deformations. During strong seismic events, such

structures can be subjected to severe damage and may become unserviceable and/or even need to be decommissioned. Superelastic SMA is a unique material, which has the potential to reduce earthquake damage significantly, while dissipating considerable amounts of energy through yielding, and regaining its original shape upon stress removal. Thus, SMA-RC structural elements are expected to remain serviceable even after strong earthquakes, thus requiring only minor repairing work. Such repaired elements are expected to sustain repeated high seismic events, which can considerably reduce post-earthquake expenditures. This study should assist structural engineers in designing smart SMA-RC connections, with a potential to mitigate post-earthquake joint repairs and enhance the overall seismic performance of RC frame structures.

3. Details of Specimens

Two ¾-scale beam-column joint specimens are considered in this study. Both are reinforced with SMA at the plastic hinge region of their beam along with regular steel in the remaining parts of the joints. One joint was an intact specimen (JBC-2), while the other was repaired (JBC-3) subsequent to damage induced by reversed cyclic loading. Both joints were constructed and tested at the Structures Laboratory of the University of Western Ontario.

3.1. Test specimens

An eight-storey RC building with moment resisting frames was designed and detailed in accordance with Canadian Standards (CSA A23.3-04). The building was assumed to be located in the western part of Canada on firm ground with un-drained shear strength of at least 100 kPa. The elevation and plan of the building are shown in Fig. 1. The moment frames were designed with a moderate level of ductility. An exterior beam-column joint was isolated at the points of contra-flexural, from the mid-height of the fifth floor to the mid-height of the sixth floor (Joint A in Fig. 1).

The size of the BCJ test specimens was reduced by a factor of ¾ to account for limitations of laboratory space and testing equipments. The forces acting on the joints were also scaled down by a factor of $(¾)^2$. This factor was chosen to maintain normal stresses in the scaled models similar to that of the full-scale joint. The beam and column were designed with the maximum moment and shear forces developed considering all code specified load combinations. The design column axial force, *P,* was 620 kN (139.5 kip) and the scaled down *P* became 350 kN (78.8 kip). The detailed design of the joints is given in Fig. 2.

The geometry, longitudinal and transverse reinforcement arrangements were similar for both specimens. The reduced cross-section of the column was 250 mm (9.84 in) by 400 mm (15.75 in) with 4-M20 (diameter: 19.5 mm or 0.77 in) longitudinal rebars corresponding to a 1.20% reinforcement ratio. The column was transversely reinforced with M10 (diameter: 11.3 mm or 0.44 in) closed rectangular ties spaced at 80 mm (3.15 in) in the joint region and for a distance of ±640 mm (25.20 in) from the face of the joint. The spacing of the ties for the remaining length of the columns was 115 mm (4.53 in).

SE SMA was used as longitudinal reinforcement at the plastic hinge region of the beam. The top and bottom longitudinal reinforcements were 2-SMA20 (diameter: 20.6 mm or 0.81 in) bars (reinforcement ratio = 1.33%). The size of SMA rebar was chosen such that the SMA section had 1% lower moment carrying capacity compared to that of steel section preventing steel bars from yielding. The plastic hinge length was calculated using the following equation proposed by Paulay and Priestley (1992) as 360 mm (14.17 in) from the face of the column (Fig. 2).

$$L_p = 0.08L + 0.022d_b f_y \quad (1)$$

where L represents the length of the member in mm, d_b represents the bar diameter in mm, and f_y is the yield strength of the rebar in MPa. Mechanical couplers were used to connect SMA rebars and regular steel rebars (Fig. 3). The total length of SMA rebars was 450 mm (17.72 in) from the centre

to centre of the coupler as shown in Figs. 2 and 3 (a), where anchoring lengths of 50 mm (1.97 in) were required at both ends. The ties of the beams were spaced at 80 mm (3.15 in) for 800 mm (31.5 in) length adjacent to the column and then spaced at 120 mm (4.72 in). The size of the longitudinal rebar and the size and spacing of the transverse reinforcement for the joint conformed to current code requirements (CSA A23.3-04).

Machining large diameter bars of Ni-Ti using conventional equipment and techniques is extremely difficult due to its high hardness. Although there are various ways of welding and soldering Ni-Ti, e.g. using e-beam, laser, resistance and friction welding, and brazing with Ag-based filler metals; welding Ni-Ti to steel is much more problematic because of the development of a brittle connection around the weld zone (Hall 2003). Threading large diameter nitinol bars reduces its strength due to its sensitivity to notches. Therefore, instead of threaded couplers, bar lock couplers with flat shear bolts have been used in this study for splicing SMA with steel rebar.

Regular single barrel type screw lock couplers (Barsplice Products Inc. 2006) have been used for connecting steel rebars and SMA rebars. They consist of smooth shaped steel sleeves with converging sides. Each end of the reinforcing bars is inserted into one of the coupler ends until it reaches the middle pin (center stop). Both rebars meet head to head separated by a pin at the middle. Screws are used to hold the rebars, which are tightened until their heads are sheared off, indicating that the required torque is reached. Figure 4 illustrates the couplers used in the reinforcement caging of JBC-2/JBC-3. The coupler was tested using a universal testing machine with SMA rebar at one end and steel rebar on the other end. To hold the rebars at their proper positions with minimum slippage, nine 5 mm (0.20 in) diameter flat end screws were found satisfactory for SMA rebar and five 5 mm (0.20 in) diameter sharp end screws for steel rebar. The test set up is shown in Fig. 4 (b). This arrangement could stress the SMA bar up to its full SE strain range with minor slippage.

3.2. Materials

3.2.1. Superelastic Shape Memory Alloy – SMAs are unique alloys with the ability to undergo large deformations and return to their original shape through stress removal (superelasticity) or heating (shape memory effect). Among a number of SMAs, Ni-Ti alloys, in particular, have distinct thermo-mechanical properties including superelasticity, shape memory effect, and hysteretic damping.

Equi-atomic Ni-Ti alloy (50-60% Nickel and 40-50% titanium) bar was used as reinforcement in the JBC-2 specimen. Its austenite finish temperature, A_f, defining the complete transformation from martensite to austenite, ranges from -15°C to -10 °C. When the temperature is above A_f, SMA will remain in the fully austenite phase. If the temperature falls below A_f, still SMA will exhibit SE behaviour as long as the temperature is above the martensite start temperature (M_s,), which is usually 10 to 30 °C lower than A_f (Alam et al. 2007a). If the temperature of SMA gets below M_s, the rebar may lose its superelasticity. Heating the rebar above A_f will allow SMA to regain its superelasticity.

Each Ni-Ti bar used in this study was 450 mm (17.72 in) long and 20.6 mm (0.81 in) in diameter. Each end of the rebar was inserted into the coupler over a length of 50 mm (1.97 in). Figure 5 shows the cyclic tensile behaviour of a Ni-Ti bar within couplers at room temperature. The characteristic stress-strain curve shows a flag-shaped response. The yield point (f_y) is identified as 401 MPa (58 ksi) and its Young's modulus (E_y) is calculated as 62.5 GPa (9031 ksi). Although SMA does not have a yielding process, yield is being used to refer to the initiation of phase transformation of SMA. Figure 5 also shows the idealized bilinear elastic-plastic SMA model with kinematic strain hardening by the dashed lines. To determine the equivalent bilinear elastic-plastic curve, the area under the stress-strain curve is calculated, and then a line having the initial slope of the curve is drawn through the origin. A second line is drawn such that the area under the two lines is equal to the area under the original curve. The yield strength is defined as the point of intersection

between the two lines and the ultimate value is considered as the maximum value of the stress in the inelastic range. Here, f_y is determined as 401 MPa, which is reached at 0.64% strain at a slope of 62.5 GPa. The rebar was tested up to a maximum of 6% strain with a residual strain of 0.73%. Since its modulus of elasticity is low compared to that of steel, it is expected to experience much higher strain than that of steel at a similar load level.

3.2.2. Concrete – The specimen was cast with highly flowable ready-mix concrete with a slump flow (inverted cone method) of 720 mm (28.35 in) in diameter. The air content of fresh concrete was 5.5%. The concrete compressive strength and split cylinder tensile strength at the time of testing were 53.7 MPa (7760 psi) and 2.8 MPa (405 psi), respectively.

3.2.3. Steel Reinforcement – Tensile strength tests of steel rebars were performed in the laboratory. The yield strength, ultimate strength, and Young's modulus of 20M reinforcing bars were 450 MPa (65 ksi), 650 MPa (94 ksi), and 193 GPa (27890 ksi), respectively. For both specimens, the steel rebars used for ties were 10M rebars with a yield strength and ultimate strength of 422 MPa (61 ksi) and 682 MPa (99 ksi), respectively.

3.2.4. Repair Concrete – The damaged specimen was repaired with flowable, shrinkage-compensated repair concrete. The concrete compressive strength and split cylinder tensile strength at the time of testing were 61.6 MPa (8900 psi) and 3.8 MPa (549 psi), respectively.

3.2.5. Epoxy – Low viscous epoxy adhesive was used to repair the cracks of JBC-3. The specified tensile strength, compressive strength, and modulus of elasticity under compression of the epoxy were 52 MPa (7510 psi), 76 MPa (10980 psi) and 1.75 GPa (253 ksi), respectively. Another type of highly workable non-sag epoxy paste was used to seal the outer face of the cracks. Its specified

tensile strength, compressive strength, and modulus of elasticity under compression were 31 MPa (4480 psi), 96 MPa (13870 psi) and 2.07 GPa (299 ksi), respectively.

3.3 Test setup and instrumentation

The BCJ specimens were tested under constant axial load (13% of its axial load capacity) that was applied at the top of the column and reversed quasi-static cyclic load applied at the beam tip. The load history applied at the beam tip was divided into two phases. It started with a load-controlled phase followed by a displacement-controlled phase. During the load-controlled phase, two load cycles were applied at 10% of the theoretical yield load (45 kN calculated from moment curvature) of the beam to verify the test setup and proper functionality of the data acquisition system. Then two load cycles were applied causing flexural cracking in the beam. This was followed by two load cycles that caused initial yielding of longitudinal rebars of the beam. Yielding of the SMA rebar was noted by observing the readings from the strain gauges. The yield load, P_y, and the yield displacement, Δ_y, were recorded. After yielding, displacement-controlled loading was applied in the form of incremental multiplies of the yield displacement, Δ_y. For each load cycle, the test specimen was subjected to two complete cycles to verify its stability. Tests were conducted up to a storey drift of 7.9% (Fig. 6), which is more than double the collapse limit as proposed by Elnashai and Broderick (1994).

The schematic diagram of the test setup is shown in Fig. 7 where the specimen is mounted in the test rig and supported by a reaction frame. The bottom of the column was hinged with pins penetrating through a sleeve with narrow holes, whereas a roller support was created at the top of the column with pins penetrating through a sleeve with 20 mm vertical slots. This slot permitted vertical deformation of the column and transmission of its axial load from the hydraulic jack to the lower hinge support. The load cycles were applied at the beam tip using an actuator, which was pin

connected at the beam-tip. The arm length was 1870 mm (73.62 in) measured from the pin connection to the mid column line.

Figure 7 also illustrates the instrumentation of the test specimens. Two load cells were used to measure the column axial load and beam tip load. During testing, displacements were measured at various locations using four linear variable displacement transducers (LVDTs). One pair of LVDT was attached to the joint area to measure the joint distortion. The other two LVDTs were placed in parallel on top and bottom of the beam at 180 mm away from the column face to measure beam rotation. A string pot was used to measure the displacement at the free end of the beam. For both BCJ specimens, electrical resistance strain gauges were installed on the main reinforcing bars and transverse reinforcement of the beam and column as shown in Fig. 3 (a). Data generated from different monitoring devices were segregated into analogue (load cells, LVDTs) and digital (strain gauges) feeds, which were connected to the data acquisition system. A portable computer attached to the data acquisition system was used to record readings at a constant time interval with one reading per second.

4. Testing and repairing of specimens

4.1 Performance of JBC-2

Figure 8 shows the load-storey drift relationship of the intact SMA-RC beam-column joint specimen JBC-2. The First Flexural Crack (FFC) was detected at the bottom of the beam at 160 mm (6.30 in) away from the column face at a drift of 0.22%. In the subsequent cycle at the same drift; another crack developed at the top of the beam at a distance of 197 mm (7.76 in) away from the column face and extended meeting the first crack. Thus, a single fine crack is formed that extended over the full beam-depth. With the progress of loading several flexural cracks occurred at the top and bottom of the beam along a length of 1300 mm (51.18 in) measured from the column face. At a beam tip-load of 18 kN (4.05 kip) and a drift of 0.66%, a small crack appeared at the bottom edge

of the joint region near the column face. A fine crack took place along the diagonal of the joint at a beam tip-load of 22 kN (4.95 kip) corresponding to a drift of 1.12%. It was observed that the bottom SMA rebar reached its yield strain at a beam tip-load of 32.7 kN (7.36 kip) and a drift of 1.97%. In this case, the corresponding yield displacement, Δ_y was found as 18 mm (0.71 in). At a deformation level of $2\Delta_y$, the existing flexural cracks started to propagate deeper into the beam. Some minor cracks streamed out of the FFC toward the column face. The FFC also started to grow wider and reached a width of 5.3 mm (0.21 in) at the outer face. When the displacement cycle reached a zero value, the crack width at the plastic hinge region became smaller and it was even less than 0.5 mm (0.02 in). At a deformation level of $3\Delta_y$, the FFC opened up to 7.4 mm (0.29 in) and later closed to a width of less than 1 mm (0.04 in). Several existing flexural cracks in the beam extended to its full depth parallel to the column face. At a deformation level of $4\Delta_y$, the cracks became wider in the plastic hinge area of the beam. The FFC opened up to 10.7 mm (0.42 in) during the loading cycle, and part of the bottom concrete cover spalled off. At the end of this cycle, the residual FFC crack width was 2.2 mm (0.09 in), whereas all other cracks in the beam had very small width. The joint region exhibited few diagonal cracks of very fine width and small length, and remained almost fully intact. Figure 9 shows the crack pattern of JBC-2.

4.2 Repairing of JBC-2

Prior to repairing the specimen JBC-2, the beam had one major crack at half beam depth away from the column face with substantial loss of cover concrete on its top and bottom face. There were also some minor cracks in the beam within the full beam depth away from the column face. The repairing technique includes the removal of damaged concrete, placing concrete grout in the removed zone, and injecting epoxy in all accessible minor cracks.

4.2.1. Removal of damaged concrete – First, all unsound and delaminated concrete around the large crack was removed; wherever there were exposed rebars and stirrups, concrete was also removed

around them such that there was a minimum of 20 mm (0.79 in) space around the reinforcement as shown in Fig. 10 (a), (b) and (c). The perimeter of the damaged concrete area was saw-cut by a diamond blade to a minimum depth of 25 mm (0.98 in) to prevent featheredges (thin sharp edge formed at the junction of two plane surfaces meeting at an acute angle) so as to avoid stress concentrations.

4.2.2. Application of repair materials – Before the placement of repair concrete, the concrete surface was mechanically abraded to remove all bond-inhibiting materials. The prepared surface was subsequently pre-soaked to a saturated surface-dry condition. A formwork (U-shaped) with an opening at one side was built at the bottom damaged part of the beam. The repair concrete was applied through the opening, and the bottom repaired part was allowed to cure for one day. The next day, all major and minor cracks were sealed with non-sag epoxy paste and three port-holes were installed on each side at three different depths to inject epoxy through them (Fig. 10 (d)). When the epoxy paste was cured, an epoxy adhesive was poured through the major crack by gravity feed as shown in Fig. 10 (e). Once the major crack was completely filled, the epoxy adhesive was injected through port-holes using standard pressure-injection equipment starting from the bottom to the upper port as shown in Fig. 10 (f). After one day of curing, a formwork (||-shaped) was built for the top damaged part of the beam, and then the repair concrete material was placed inside the formwork. Both top and bottom parts of the repair concrete were then cured for 7 days. The cost of epoxy injection repair was roughly $13 CAD per linear 100 mm (3.94 in), which included both material and labour costs. A 22.7 kg (50 lb) bag of repair concrete material was required for repair and its price was approximately $50 CAD. It required 6 hours of labour involving one operator for removing delaminated concrete and 4 hours involving two operators for preparing formwork and placing new concrete.

4.3 Performance of JBC-3

The behaviour of specimen JBC-3 was found similar to that of JBC-2. Figure 11 shows its beam tip load versus storey drift relationship. The first flexural crack (FFC) was observed at the top of the beam at a distance of 250 mm (9.84 in) away from the column face at a beam tip-load of 14.5 kN (3.26 kip) corresponding to a drift of 0.52%. In the very next cycle at the same drift, another crack developed at the bottom of the beam at a distance of 170 mm (6.69 in) away from the column face and extended meeting the first crack. Thus, a single fine crack was formed that extended over the full beam-depth. The FFC did not occur at the cold joint region, but rather took place at the middle of the repaired section as shown in Figs. 12 (b) and 13. This indicates the excellent bonding between the old and new concrete. Additional cracks occurred along the beam length with the progress of loading. The joint region was almost fully intact with very few cracks of fine width. The top longitudinal rebar of the beam first yielded at a beam tip-load of 42.7 kN (9.61 kip) with a corresponding yield displacement, Δ_y of 18 mm (0.71 in, drift of 1.97%). As the loading increased, the FFC started to grow wider. At 3.3% drift, the FFC became 6 mm (0.24 in) wide at the top, while in the reversed direction at the same drift, the crack size was 4 mm (0.16 in) at the bottom. At a displacement of $3.3\Delta_y$ (6.6% drift), the specimen suffered a 10 mm (0.39 in) wide crack at the top, and a 9 mm (0.35 in) crack at the bottom while in the reversed direction. At this stage, unloading could close the crack to 2 mm (0.08 in) at the top. The residual crack at the bottom was found a bit wider, which is 3 mm (0.12 in). At a displacement ductility of $4\Delta_y$ (7.9% drift), the FFC at the top became 19 mm (0.75 in) wide whereas the bottom experienced a 16 mm (0.63 in) wide crack. At this stage, some concrete cover from the top and bottom part of the beam started to spall off and the stirrups at the repaired section became visible. Throughout the test, the axial load of the column was maintained and the joint area remained fully undamaged apart from a few hairline cracks (Fig. 12).

5. Performance comparison between JBC-2 and JBC-3

Based on the material properties reported in 'Materials' section, the axial compressive load of the column was calculated as 2490 kN (560.3 kip). The theoretical beam moment capacities of JBC-2 and JBC-3 were calculated by using the actual material properties of the units at the face of the column as 99.5 kN.m (73.4 kip.ft) and 100.3 kN.m (74.0 kip.ft), respectively. The column flexural capacity was calculated by using the column interaction diagram as 135.1 kN.m (99.7 kip.ft) for the specific axial compressive load (350 kN, 78.8 kip) applied during the test. The flexural strength ratio of columns to beam is calculated as 2.7, which satisfies the strong-column weak-beam design philosophy. The joint shear strength was also determined, which is 1042 kN (234.5 kip). This section compares the performance of JBC-2 and JBC-3 in terms of their load-storey drift envelope, cumulative energy dissipation capacity, and strains in rebar.

5.1 Load-storey drift envelope

Figure 14 shows the beam-tip load versus storey drift envelope of the two tested specimens JBC-2 and JBC-3. Both envelopes exhibited typical elasto-plastic behaviour. They started with comparable initial stiffness and followed a similar trend. In the case of JBC-2, the load continuously increased with the increase of the storey-drift without showing any reduction in load-carrying capacity. On the other hand, JBC-3 showed a gradual decline in load carrying capacity beyond a storey-drift of 6.5%. However, JBC-3 could reach a peak load of 0.3% larger than that of JBC-2. Both specimens maintained a stable post-yield load carrying capacity throughout the test. At the final test stage of 7.9% drift, the beam tip-load of JBC-3 was only 5.2% lower compared to that of JBC-2. In the case of JBC-2 the stiffness degradation in consecutive cycles varied from 5% to 19% whereas in the case of JBC-3 the stiffness degradation was observed as 3% to 25%.

5.2 Cumulative energy dissipation

The cumulative energy dissipation by the beam-column joint specimens during reversed cyclic loading was calculated by summing up the dissipated energy in successive load-displacement loops throughout the test. The cumulative energy dissipation with respect to storey drift for specimens JBC-2 and JBC-3 is presented in Fig. 15. JBC-3 dissipated 2.0 kN.m (1.48 kip.ft) of energy at a storey drift of 3% (collapse limit as defined by Elnashai and Broderick 1994), which is 11.5% smaller than that of JBC-2 at the same amount of drift. The amount of energy dissipated at 4% storey drift for JBC-2 is equivalent to the amount of energy dissipated by JBC-3 at a storey drift of 4.2%. At a storey-drift of 7.9%, JBC-2 was found to absorb 16.7 kN.m (12.32 kip.ft) of energy, whereas JBC-3 dissipated 16.5 kN.m (12.18 kip.ft) of energy at the same storey-drift, which is only 1.2% smaller than that of JBC-2. Thus, it is evident that the repaired specimen JBC-3 could dissipate an almost equal amount energy to that of the original specimen, JBC-2. However, the level of damage of the cover concrete in JBC-3 was relatively larger in the beam hinge region (Figs. 9 and 12) than that of JBC-2.

5.3 Strains in rebars

Strains were measured in longitudinal and transverse reinforcing bars. Figures 16 (a) and (b) show the measured strains in the main bottom reinforcing SMA rebar at the plastic hinge region, close to the column face of specimens JBC-2 and JBC-3, respectively. Figure 16 (b) shows that specimen JBC-3 suffered a higher residual strain in the SMA bar compared to that of JBC-2 (Fig. 16 (a)). This accumulation of residual strain resulted from repetitive cycles of loading. For specimen JBC-2 the measured strain in the main steel reinforcing bar inside the joint varied from +1156 to -86 micro-strains (absolute range: 1242 micro-strain, Fig. 17 (a)), whereas the steel reinforcing bar inside the joint of specimen JBC-3 experienced +611 to -697 micro-strains (absolute range: 1308 micro-strain, Fig. 17 (b)). The measured strain in the transverse reinforcement inside the joint of JBC-2 varied from +990 to -24 micro-strains (range: 1014 micro-strain, Fig. 18 (a)), while the corresponding values for specimen JBC-3 were +848 to -132 micro-strains (range: 980 micro-strain, Fig. 18 (b)).

Although the range of strains for JBC-2 and JBC-3 is comparable, the difference in distribution might be due to the pre-straining of steel rebars in the repaired specimen, JBC-3 during loading of the original specimen, JBC-2.

5.4 Plastic hinge length

The plastic hinge length, L_p of a structural member is an essential parameter in evaluating the response of a structure and its damage due to seismic and/or other loads. Beam tip displacement test data from reversed cyclic loading of beam-column joint specimens were used to determine the equivalent plastic hinge lengths (Park and Paulay, 1975). From the force-displacement and moment-curvature test results, bilinear elastic perfectly plastic models have been used to obtain the yield and ultimate values of displacement and curvature (Alam et al. 2008). The following equation can be solved to determine the experimental value of L_p.

$$\Delta_u - \Delta_y = \left(\phi_u - \phi_y\right) L_p \left(L - \frac{L_p}{2} \right) \qquad (2)$$

where, Δ_y and Δ_u represent the yield and ultimate beam tip displacement from test data, and φ_u and φ_y represent the yield and ultimate curvature values, respectively and L is the beam length. A numerical model proposed for estimating L_p by Paulay and Priestley (1992) as presented in Eq. 1 was also used to determine L_p. The values of L_p of both specimens are presented in Table 1. The results indicate that the prediction obtained from Eq. 1 could estimate the plastic hinge length of SMA RC BCJ with reasonable accuracy.

6. Comparison of performance between steel and SMA RC BCJs

There is a great potential for utilizing SMA as concrete reinforcement, however, the cost of this material is a major restraining factor to its implementation. Although there has been a substantial reduction in the price of Ni-Ti over the last ten years, from more than 1000 USD to below 80 USD per kg at present, the price is still considerably higher than that of other construction materials.

Nevertheless, SMA can be used along with steel in a hybrid system, thus achieving a cost competitive design with several performance gains.

Screw lock couplers used for connecting SMA with steel have several advantages over threaded couplers since they can be applied readily with no requirements of threading or specially treating the bars. No special installation equipment is required; quick and easy installation save time and money, which is ideal for new construction.

Youssef et al (2008) tested a ¾-scale steel RC beam-column joint (JBC-1) under reversed cyclic loading, which had similar dimensions and reinforcement arrangements and was subjected to similar drifts to those of JBC-2 and JBC-3. Figure 19 shows the load-storey drift relationship of JBC-1 and Table 2 presents various performance parameters of JBC-1 in comparison to those of JBC-2 and 3. The result shows that it had similar load carrying capacity to those of JBC-2 and JBC-3, which is 1.7% and 6.1% smaller compared to that of JBC-2 and JBC-3, respectively. However, JBC-1 suffered much larger residual drift (average 4.43%), compared to those of JBC-2 (average 1.42%) and JBC-3 (average 1.36%) after 8% drift. Due to larger hysteretic curves, JBC-1 dissipated 37% and 38% higher energy compared to that of JBC-2 and JBC-3, respectively. In case of JBC-1, the specimen experienced extensive cracking at the face of the column and over a length of 300 mm of the beam whereas the joint region was fully intact. In case of JBC-2 and JBC-3, SMA bars were placed close to the face of the column and its low modulus of elasticity compared to that of steel resulted in higher strain in the plastic hinge region, causing a major crack away from the column face. The bottom steel rebar of JBC-1 suffered a high residual strain of more than 6000 micro-strain, whereas the SMA reinforced JBC-2 and JBC-3 specimens suffered residual strains of less than 1000 and 2000 micro-strain, respectively (note that JBC-3 was tested twice and its residual strain is cumulative of the two tests). Since the beam reinforcements of JBC-1 at the column face were highly damaged with large residual strain, repairing such a specimen would require replacing

damaged rebars, besides epoxy repairing of other damage. This would involve removing concrete not only from the beam, but also from the joint region. If this is the case in a real RC frame structure, it would affect the column axial capacity, and extra support may be required to carry the axial load and transfer it to lower members. Other options for repairing such joints include steel jacketing, application of external steel elements or externally bonded fiber reinforced polymer (FRP) composites. Although the initial cost of conventional steel RC frames would be lower by 10 to 20% compared to that of SMA RC frames with SMA placed only at the hinging regions of beams, the strengthening techniques for steel RC beam-column joints would be 3 to 5 times more costly, laborious and time consuming compared to that of the simple technique required for repairing the damaged specimen JBC-2. Again, although SE SMA RC BCJs dissipate lower amount of energy compared to that of steel RC BCJ, its advantage lies in its ability to dissipate considerable amounts of energy through inelastic deformation of SMA rebar and potentially recover most of its deformation, requiring only minimum repairing effort in terms of material, labor, cost and time.

7. Conclusions and Future Recommendations

This paper discusses a novel and smart approach for reducing the seismic vulnerability of RC frame structures by utilizing a smart material, Ni-Ti shape memory alloy, in beam-column joints. The use of superelastic SMA rebars in the plastic hinge region of a beam-column joint has been examined under reversed cyclic loading. Based on the experimental observations and analysis of test results, the following conclusions can be drawn.

1. The flag-shaped hysteretic stress-strain curve of SE SMA rebar produced a nearly flag-shaped force-displacement hysteresis for both the original (JBC-2) and repaired (JBC-3) beam-column joints under reversed cyclic loading. This resulted in very small residual displacements in both specimens. This extraordinary characteristic of SE SMA-RC BCJs could have a great benefit in highly seismic areas, where such RC joints would remain functional even after a strong earthquake;

2. The joint region and the column of both specimens (original and repaired) did not experience any damage, since the specimens were designed and detailed according to current seismic codes.

3. The damaged SE SMA-RC BCJ repaired with commercially available structural repair concrete performed satisfactorily with no reduction in load carrying capacity compared to that of the original specimen;

4. The repaired BCJ specimen JBC-3 could dissipate an amount of energy comparable to that of the original specimen JBC-2;

5. The longitudinal SMA rebar of specimen JBC-2 experienced negligible residual strain, while the longitudinal SMA rebar of specimen JBC-3 suffered some residual strain because of repetitive cyclic deformation. The steel rebars and transverse reinforcements inside the joint of specimen JBC-2 and JBC-3 experienced equal amounts of absolute strains, while their distribution was different because of the pre-straining of steel rebars and stirrups during the loading of JBC-2;

6. The plastic hinges were formed at a distance away from the column face for both the original and repaired specimens. The plastic hinge lengths for SMA RC beam-column joints were determined experimentally. The Paulay and Priestley equation (1992) was found to predict the plastic hinge length of SMA RC BCJs with reasonable accuracy;

This study mainly focused on constructing a smart structural element consisting of a steel RC subassembly with SMA bar at its beam plastic hinge region, and observing its performance and the associated level of damage under reversed cyclic loading, in both its original and repaired states. The test results will be used in developing a numerical model, which can simulate the performance of original and repaired SE SMA-RC beam column joints. Such a model can be extended to assess the performance of repaired SE SMA-RC multi-storey frames under dynamic loading, allowing predicting their capacities and meeting seismic resistance requirements. Future research will investigate the seismic performance of SE SMA RC beam-column connections with a slab and

transverse beams. Extensive research is also needed to establish proper guidelines for the utilization of SMA-steel coupled reinforcement in RC frame structures, before any large scale implementation of the proposed construction method. Additional research is also necessary to examine design code provisions for the seismic design of RC structures considering the low modulus of elasticity, low energy dissipation capacity, large deformation capability, negligible residual strain, and recentering capability of SMA compared to that of steel. Further study is also required to adequately describe the relationship between various damage states, demand (inter-storey drift or beam rotations) on such new structural components and its associated retrofitting costs, which will be useful for the purpose of damage assessment of buildings after an earthquake.

ACKNOWLEDGMENTS

The authors gratefully acknowledge the donation of SE SMA bars from ATI Wah Chang Inc, Albany, OR and the repair materials from BASF Construction Chemicals and BASF Building Systems, ON, Canada. Thanks are also due to A-1 Restoration, London, ON, Canada for their assistance in repairing the specimen. Sustained financial support by the Natural Sciences and Engineering Research Council of Canada has been critical for conducting this research.

REFERENCES

Alam, M. S.; Youssef, M. A.; and Nehdi, M., 2008, "Analytical Prediction of the Seismic Behaviour of Superelastic Shape Memory Alloy Reinforced Concrete Elements," *Engineering Structures, Elsevier,* V. 30, No. 12, 2008, pp. 3399-3411.

Alam, M. S.; Youssef, M. A.; and Nehdi, M., 2007a, "Utilizing Shape Memory Alloys to Enhance the Performance and Safety of Civil Infrastructure: a Review," *Canadian Journal of Civil Engineering*, V. 34, No. 9, Sept. 2007, pp. 1075-1086.

Alam, M. S.; Nehdi, M.; and Youssef, M. A., 2007b, "Shape Memory Alloy-Based Smart RC Bridge: Overview of State-of-the-Art", *Smart Structures and Systems*, V. 4, No. 3, pp. 367-389.

Alam, M. S.; Youssef, M. A.; and Nehdi, M., 2007c, "Seismic Behaviour of Concrete Beam-Column Joints Reinforced with Superelastic Shape Memory Alloys", *9th Canadian Conference on Earthquake Engineering*, June 2007, ON, Canada, Paper no. 1125, 10 p.

Alam, M. S.; Nehdi, M.; and Youssef, M. A., 2007d, "Applications of Shape Memory Alloys in Earthquake Engineering", 9th *Canadian Conference on Earthquake Engineering,* June 2007, ON, Canada, Paper no. 1124, 10 p.

Alam, M. S.; Youssef, M. A.; and Nehdi, M., 2005, "Shape Memory Alloys as a New Construction Material", *Proceedings of Cansmart 2005 - the 8th International Workshop on Smart Materials and Structures*, October 13-14, Toronto, ON Canada, pp. 123-132.

Barsplice Products Inc., 2006, "Zap Screwlok ® Mechanical Splices and Connectors for Reinforcing Bars – Review," accessed on April 08, 2006, available at: http://www.barsplice.com/BPI_Scans/Zap_Data-Sheet_RevA.pdf.

CSA A23.3-04, 2004, *Design of Concrete Structures,* Canadian Standards Association, Rexdale, ON, Canada.

Elnashai, A. S., and Broderick, B. M., 1994, "Seismic Resistance of Composite Beam-Columns in Multi-Storey Structures. Part 1: Experimental Studies," *Journal of Constructional Steel Research*, V. 30, No. 3, pp. 201-229.

Elnashai, A. S., V. Papanikolaou, and D. H. Lee, 2008. ZEUS-NL Version 1.8.1, User Manual, *Mid-America EarthquakeCenter (MAE) Report*.

Engindeniz, M.; Kahn, L. F.; and Zureick, A.-H., 2005, "Repair and Strengthening of Reinforced Concrete Beam-Column Joints: State of the Art," *ACI Structural Journal*, V. 102, No. 2, Mar.-Apr. 2005, pp. 1-14.

Hall, P. C., 2003, "Laser Welding Nitinol to Stainless Steel," *Proc. of the International Conference on Shape Memory and Superelastic Technologies*, California, pp. 219-228.

Mander J.B., Priestley M.J.N. and Park R., 1988, "Theoretical stress-strain model for confined concrete," *Journal of Structural Engineering*, V. 114, No. 8, pp. 1804-1826.

NBCC 2005, National Building Code of Canada, 2005, National Research Council, Canada.

Park, R., and Paulay, T., 1975, *Reinforced Concrete Structures,* John Wiley & Sons Inc, New York, 769p.

Paulay, T., and Priestley, M. N. J., (1992) *Seismic Design of Reinforced Concrete and Masonry Buildings,* John Wiley & Sons, Inc., New York, 744p.

Parra-Montesinos, G. J., Peterfreund, S. W., and Chao, S.-H., 2005, "Highly Damage-Tolerant Beam-Column Joints Through Use of High-Performance Fiber-Reinforced Cement Composites," *ACI Structural Journal*, V. 102, No. 3, pp. 487-495.

Saatcioglu, M.; Mitchell, D.; Tinawi, R.; Gardner, N. J.; Gillies, A. G.; Ghobarah A.; Anderson, D. L.; and Lau, D., 2001, "The August 17, 1999, Kocaeli (Turkey) Earthquake-Damage to Structures," *Canadian Journal of Civil Engineering*, V. 28, No. 4, pp. 715-737.

Said A.M. (2009), "Damage characterization of beam-column joints reinforced with GFRP under reversed cyclic loading", Smart Structutes and Systems, 5(4), 443-455.

Saiidi, M. S., and Wang, H., 2006, “Exploratory Study of Seismic Response of Concrete Columns with Shape Memory Alloy Reinforcement,” *ACI Structural Journal*, V. 103, No. 3, pp. 436-443.

Wilson, J. C., and Wesolowsky, M. J., 2005, “Shape Memory Alloys for Seismic Response Modification: a State-of-the-Art Review,” *Earthquake Spectra*, V. 21, No. 2, pp. 569-601.

Youssef, M. A.; Alam, M. S.; and Nehdi, M., 2008, “Experimental Investigation on the Seismic Behaviour of Beam-Column Joints Reinforced with Superelastic Shape Memory Alloys,” *Journal of Earthquake Engineering*, V. 12, No. 7, pp. 1205-1222.

Uma, S.R. and Jain, S.K. (2006), "Seismic design of beam-column joints in RC moment resisting frames - Review of codes", Struct. Eng. Mech., 23(5), 579-597.

TABLES AND FIGURES

List of Tables:

List of Figures:

Fig. 8 – Beam-tip load-storey drift relationship of specimen JBC-2.

Fig. 9 – Crack pattern of specimens after being subjected to cycles up to 72 mm (2.83 in): (a) front face of JBC-2; and (b) rear face of JBC-2.

Fig. 10 – Repairing of damaged JBC-2: (a) damaged concrete removed; (b) checking adequate spacing behind the bottom part of stirrup; (c) checking adequate spacing behind the top part of the stirrup; (d) sealing of the exterior face of the cracks; (e) gravity feed of epoxy adhesive in the major crack; and (f) injecting epoxy adhesive using pressure-injection equipment.

Fig. 11 – Beam-tip load-storey drift relationship of specimen JBC-3.

Fig. 12 – Crack pattern of specimens after being subjected to cycles up to 72 mm (2.83 in): (a) front face of JBC-3; and (b) rear face of JBC-3.

Fig. 13 – Bonding between old and new concrete.

Fig. 14 – Beam tip-load versus storey drift envelope of the specimens JBC-2 and JBC-3.

Fig. 15 – Cumulative energy dissipation-storey drifts relationship of specimens JBC-2 and JBC-3.

Fig. 16 – Strains in main longitudinal reinforcements at the column face of joint specimens: (a) JBC-2; and (b) JBC-3.

Fig. 17 – Strains in steel inside the joint of specimens: (a) JBC-2; and (b) JBC-3.

Fig. 18 – Strains in transverse reinforcement inside the joint of specimens: (a) JBC-2; and JBC-3.

Fig. 19 – Beam-tip load-storey drift relationship of specimen JBC-1 (Youssef et al. 2008).

Table 1–Calculation of plastic hinge length

Specimen	Δ_y	Δ_u	φ_y	φ_u	L_p (Eq 2)	L_p (Eq 1)
	mm (in)	mm (in)	rad/km (rad/mile)	rad/km (rad/mile)	mm (in)	mm (in)
JBC-2	18 (0.71)	72 (2.83)	22.0 (35.40)	122.0 (196.30)	374 (14.72)	312 (12.28)
JBC-3	18 (0.71)	72 (2.83)	22.7 (36.50)	129.7 (208.70)	346 (13.62)	

Table 2–Comparative results of the specimens JBC-1, JBC-2 and JBC-3

Performance parameter	JBC-1	JBC-2	JBC-3
Drift at first flexural crack (%)	0.22	0.22	0.52
First flexural Crack Load (kN)	11.7	10.5	14.5
Drift at full depth crack (%)	2.60	0.22	0.52
Yield load (kN)	51.3	32.7	42.7
Drift at yield load (%)	1.30	1.97	1.97
Average load at 5% drift (kN)	62.0	62.2	67.8
Residual drift after 5% drift (%)	2.73	0.66	0.44
Average load at 8% drift (kN)	64.7	65.9	63.2
Residual drift after 8% drift (%)	4.43	1.42	1.36

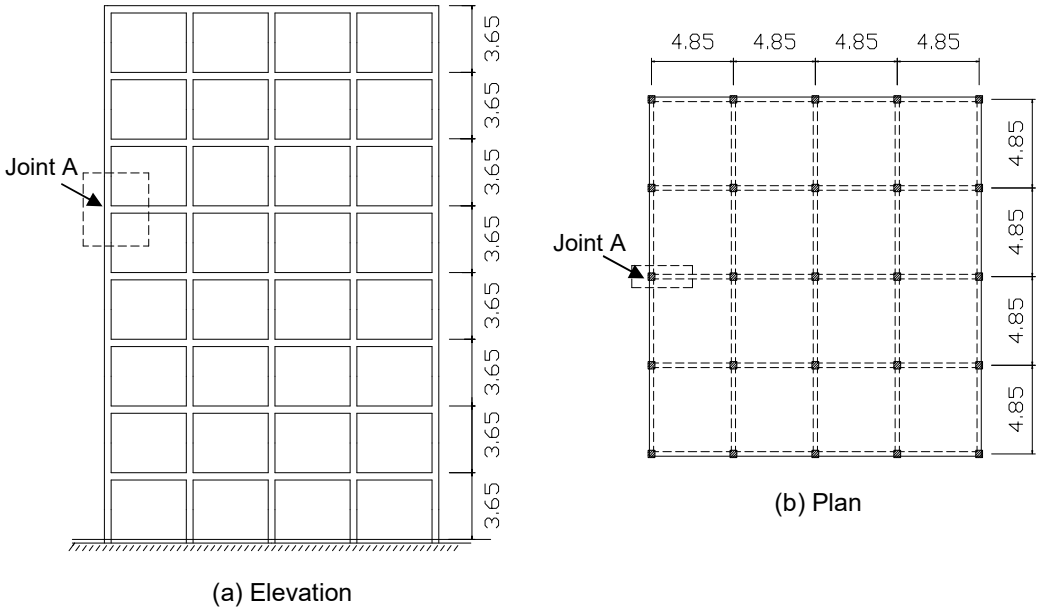

Fig. 1 – Eight-storey frame building located in the western part of Canada (dimensions in meters; 1 m = 39.37 in).

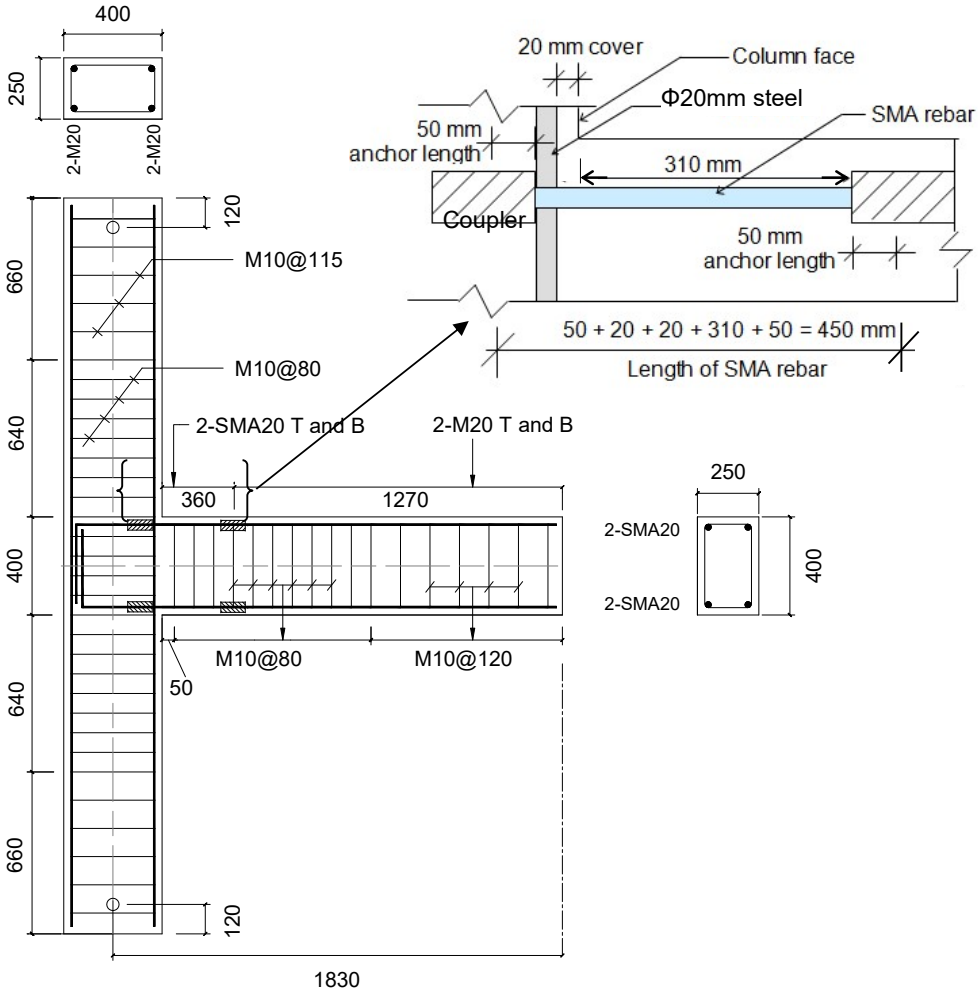

Fig. 2 – Reinforcement details of JBC-2 and JBC-3 (all dimensions in mm; 25.4 mm = 1 in).

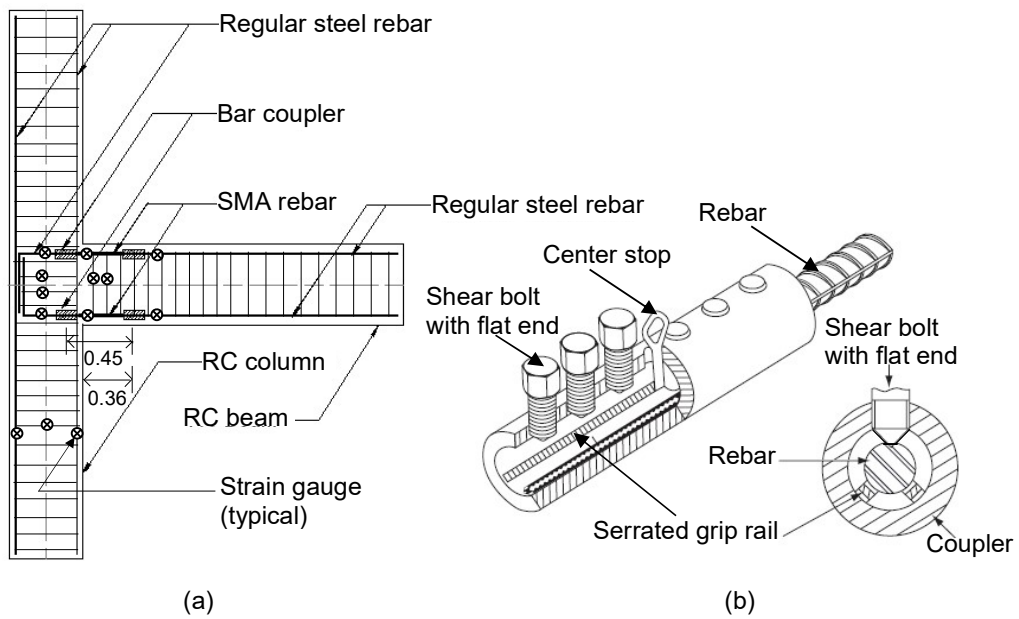

Fig. 3 – (a) Splice details of specimen JBC-2 and the positions of strain gauges; (b) regular single barrel screw-lock coupler for connecting SMA rebar with regular steel rebar (all dimensions in m; 1m = 39.37 in).

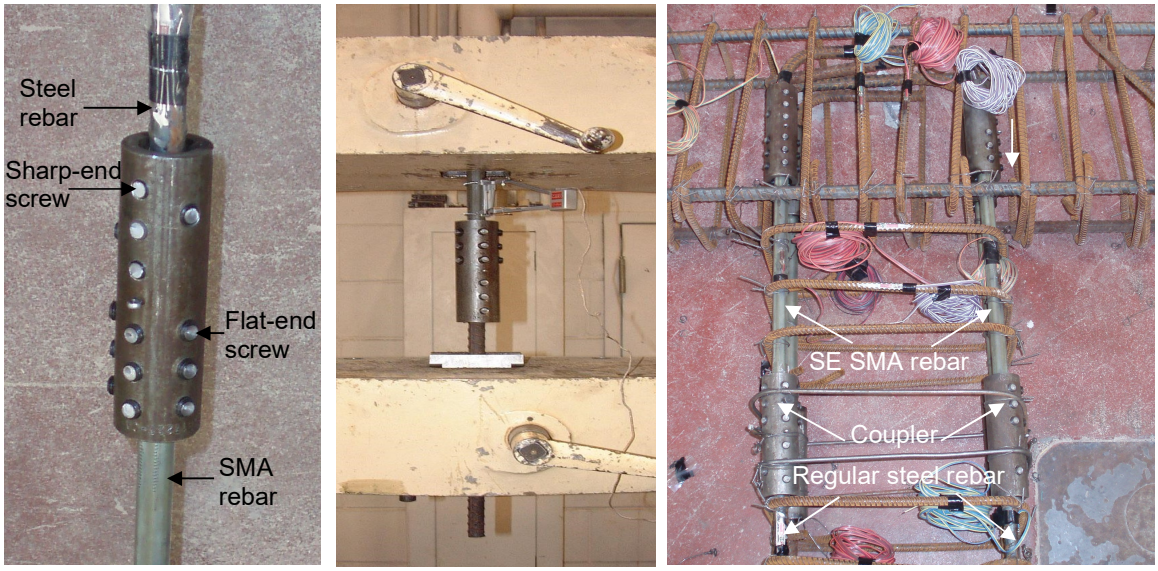

Fig. 4 – (a) Coupler used in BCJ specimens; (b) test setup of coupler in universal testing machine; and (c) reinforcement caging of BCJs.

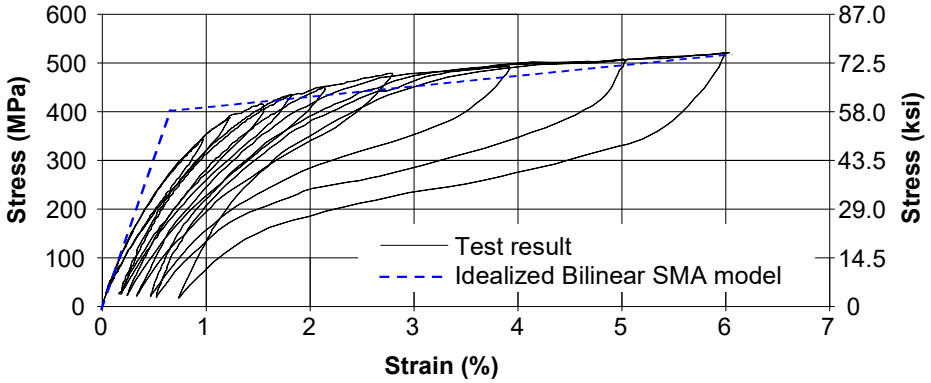

Fig. 5 – Cyclic tensile strength of SE SMA rebar within couplers.

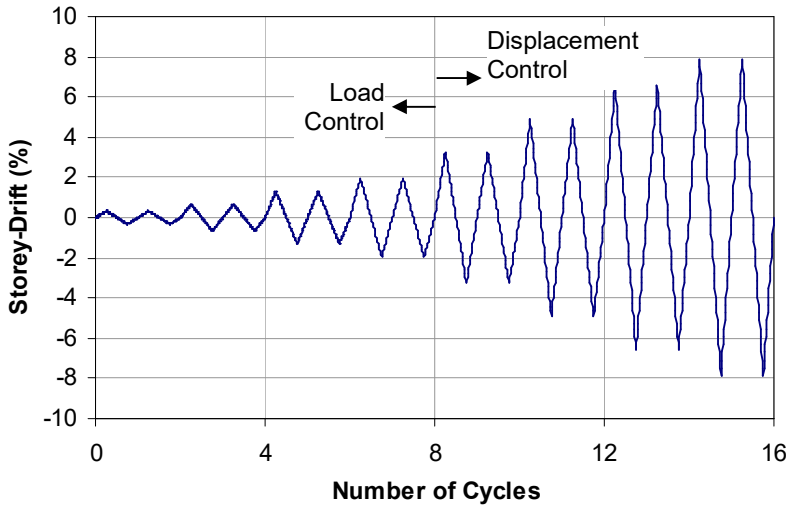

Fig. 6 – Load history for the reversed cyclic load test.

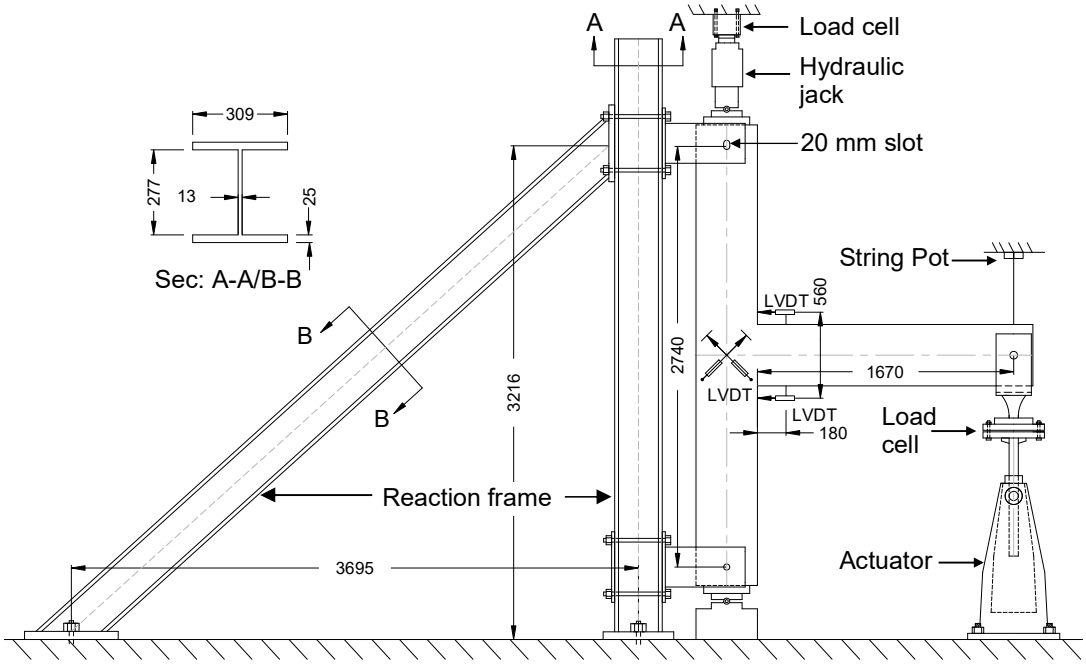

Fig. 7 – Test setup (all dimensions in mm; 25.4 mm = 1 in).

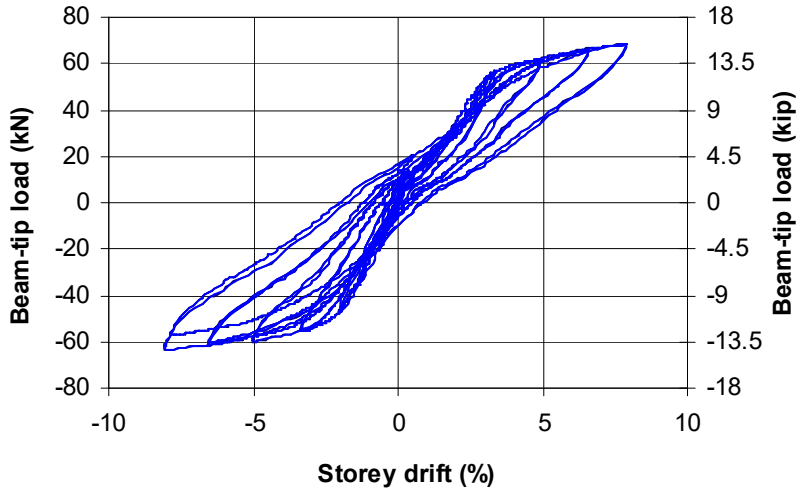

Fig. 8 – Beam-tip load-storey drift relationship of specimen JBC-2.

(a) (b)

Fig. 9 – Crack pattern of specimens after being subjected to cycles up to 72 mm (2.83 in): (a) front face of JBC-2; and (b) rear face of JBC-2.

Fig. 10 – Repairing of damaged JBC-2: (a) damaged concrete removed; (b) checking adequate spacing behind the bottom part of stirrup; (c) checking adequate spacing behind the top part of the stirrup; (d) sealing of the exterior face of the cracks; (e) gravity feed of epoxy adhesive in the major crack; and (f) injecting epoxy adhesive using pressure-injection equipment.

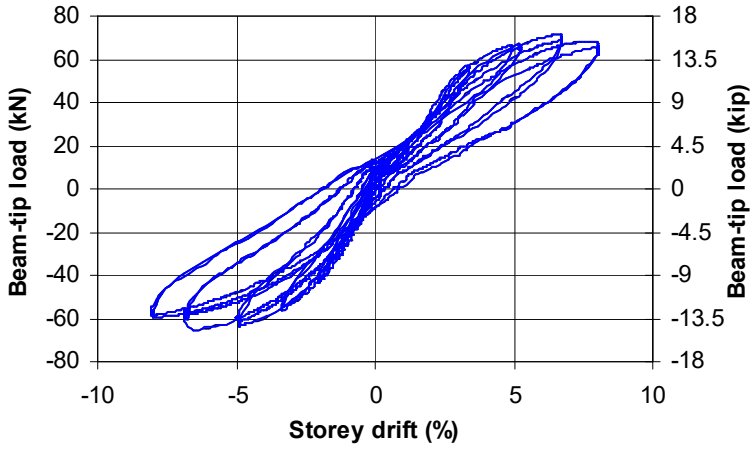

Fig. 11 – Beam-tip load-storey drift relationship of specimen JBC-3.

(a) (b)

Fig. 12 – Crack pattern of specimens after being subjected to cycles up to 72 mm (2.83 in): (a) front face of JBC-3; and (b) rear face of JBC-3.

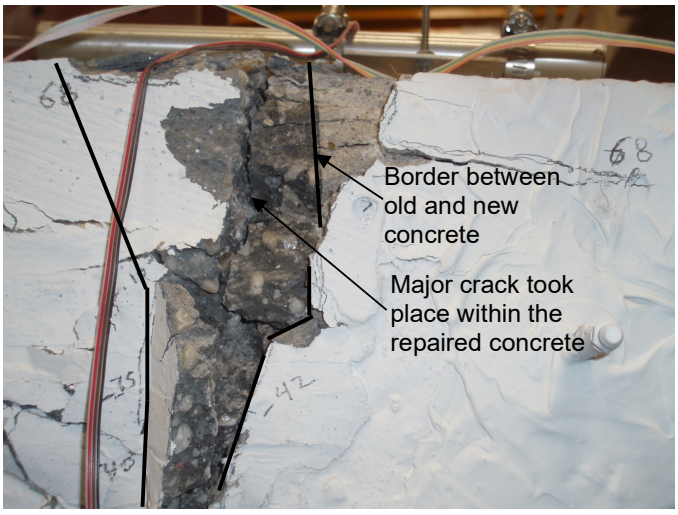

Fig. 13 – Bonding between old and new concrete.

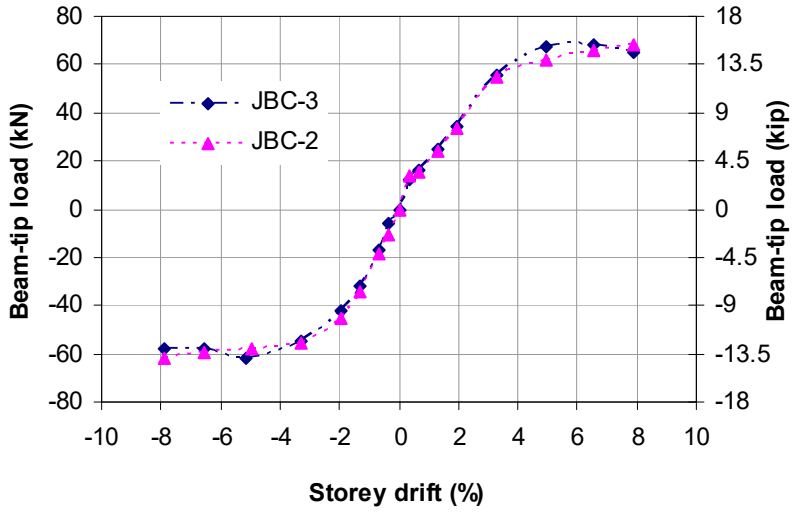

Fig. 14 – Beam tip-load versus storey drift envelope of the tested specimens JBC-2 and JBC-3.

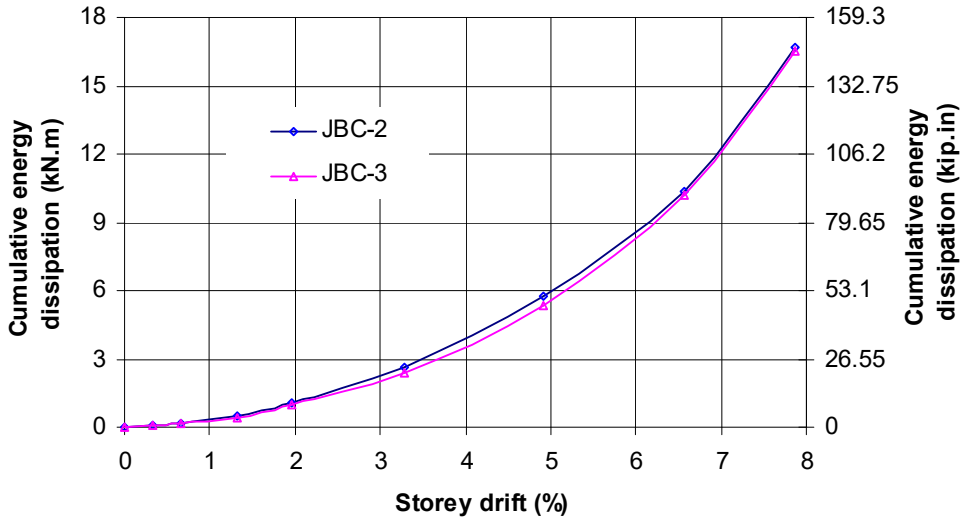

Fig. 15 – Cumulative energy dissipation-storey drifts relationship of specimens JBC-2 and JBC-3.

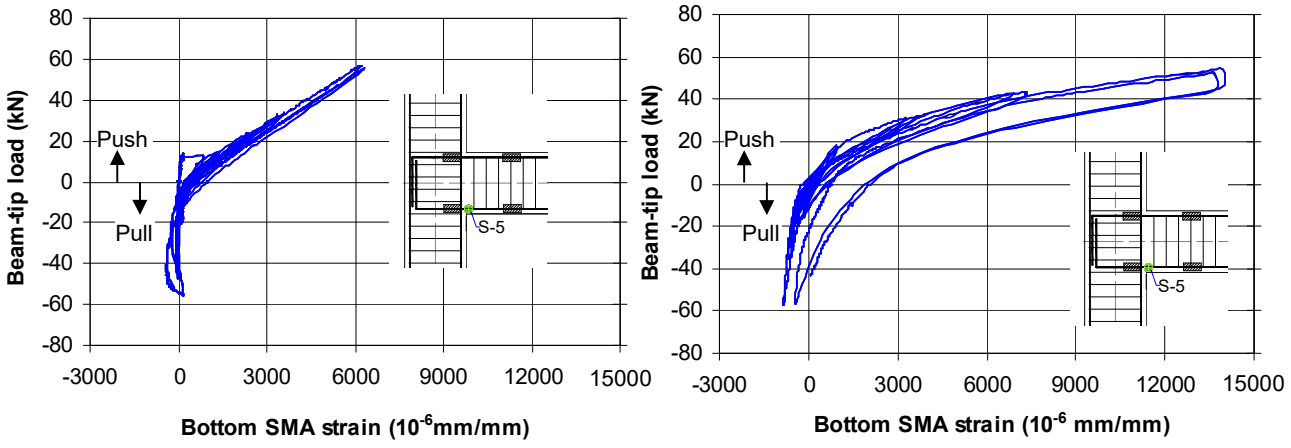

(a) (b)

Fig. 16 – Strains in main longitudinal reinforcements at the column face of joint specimens: (a) JBC-2; and (b) JBC-3.

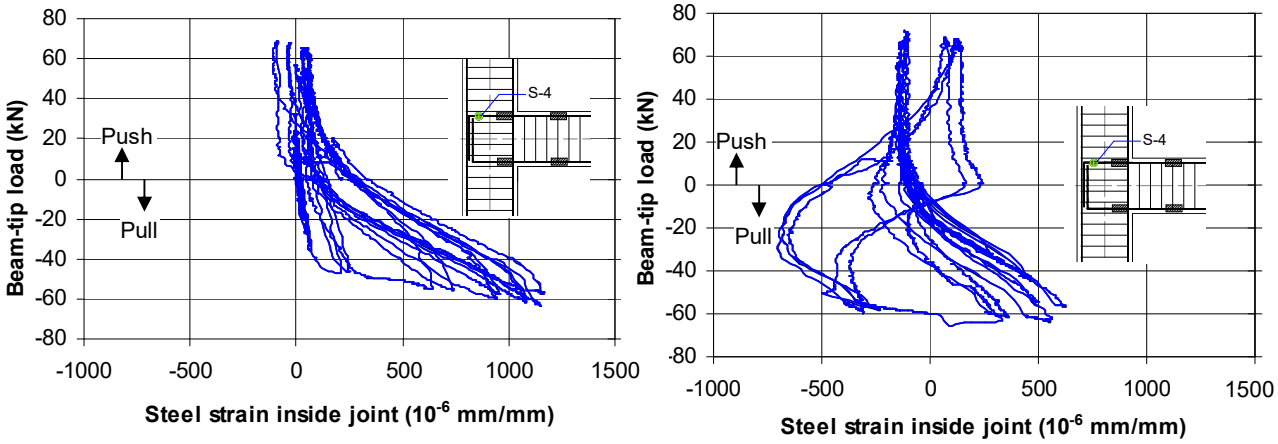

(a) (b)

Fig. 17 – Strains in steel inside the joint of specimens: (a) JBC-2; and (b) JBC-3.

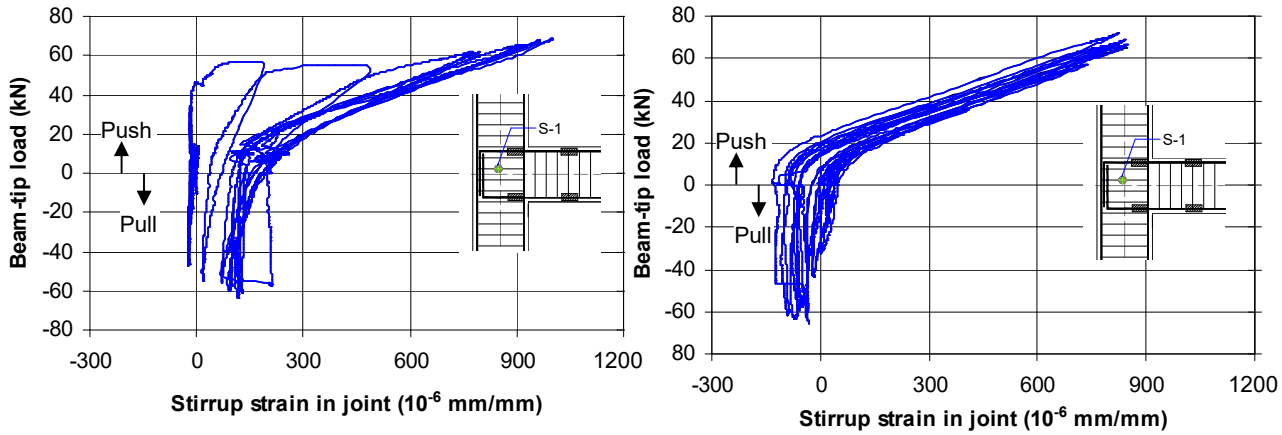

Fig. 18 – Strains in transverse reinforcement inside the joint of specimens: (a) JBC-2; and JBC-3.

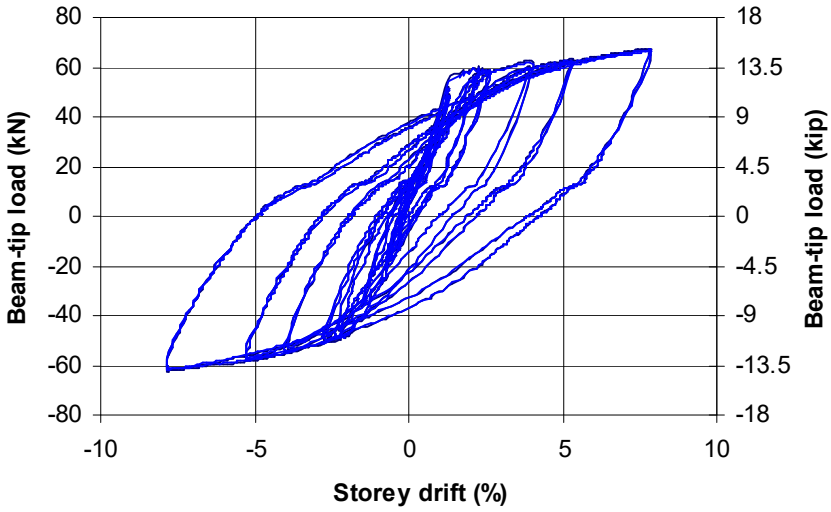

Fig. 19 – Beam-tip load-storey drift relationship of JBC-1 (Youssef et al. 2008).